Chemical Engineering Journal 102 (2004) 51–59

Chemical Engineering Journal

www.elsevier.com/locate/cej

Influence of the gas distributor on the local hydrodynamic behavior of an external loop airlift reactor

Jing Lin, Minghan Han, Tiefeng Wang, Tongwang Zhang, Jinfu Wang*, Yong Jin

Department of Chemical Engineering, Tsinghua University, Beijing 100084, China

Received 27 September 2003; accepted 24 January 2004

Abstract

The local hydrodynamic behaviors, including the gas holdup, bubble size and bubble rise velocity were measured in an external loop airlift reactor (EL-ALR) with two types of distributor—porous sinter plate and perforated plate, using an optic fiber probe. The radial and axial evolutions of these parameters and the influence of the gas distributor on the flow hydrodynamics were studied. Core-peaking and wall-peaking radial profiles of the gas holdup were found in the experiments corresponding to different bubble sizes. A mechanism model based on the assumption of the equilibrium of lateral forces acting on a bubble was proposed to interpret the different radial profiles of the gas holdup.

Keywords: Airlift reactor; Bubble behavior; Local hydrodynamics; Radial profile; Distributor; Axial evolution

1. Introduction

External loop airlift reactors (EL-ALRs), which can be used in bioprocesses, waste water treatment and chemical industry, have become increasingly popular in recent decades. Their advantages can be summarized as follows: simple construction without internals or moving parts, good heat and mass transfer capacity and good mixing properties with low energy consumption as the gas phase in the reactor serves the dual functions of aeration and agitation.

Although much work has been carried out in EL-ALRs, the proper design and scale-up of an EL-ALR still remain difficult due to the complex hydrodynamic behavior and the remarkable influence of the reactor structures on the hydrodynamics in a multiphase flow [1]. Work has been done to investigate the influence of the cross-section ratio of downcomer to riser [2,3], reactor height [1,4], gas–liquid separator configuration [5], and gas distributor type and location [6]. However, most of the previous work on EL-ALRs, including those focusing on the hydrodynamics, studied only the global parameters, such as the liquid circulation velocity [7–10] and the average gas holdup in the riser [11–14]. The local hydrodynamic behavior, which is important for a better understanding of the reactor, was less investigated. Furthermore, the detailed experimental data of the local hydrodynamics is essential for validating CFD simulations.

Up to now, only Young et al. [15], Utiger et al. [16] and Vial et al. [17] investigated the local hydrodynamics in an EL-ALR. However, they did not obtain the wall-peaking profile of gas holdup as in a vertical two-phase pipe flow in which a porous plate distribution was used the gas flow rate and the liquid flow rate could be controlled separately [18,19]. The difference is attributed to the gas distributor which has a remarkable influence on the hydrodynamics in an airlift reactor [15,20]. Young et al. [15] used a ring sparger with holes of 3.3 mm in diameter; Utiger et al. [16] used eight parallel tubes pierced with 55 holes of 0.6 mm in diameter, and Vial et al. [17] used a sparger with of 60 orifices of 1 mm in diameter. All these distributors did not distribute the gas phase very well, therefore it is necessary to use a porous distributor with much smaller holes to generate small and uniform bubbles [22].

In this work, two different types of gas distributor, namely a porous sinter plate and a perforated plate, were used to study the influence of the distributor on the hydrodynamic behavior. The local parameters of the gas phase, including the radial and axial evolution of the gas holdup, bubble size, and bubble rise velocity, were measured with an optic fiber probe. A model was proposed based on the equilibrium of the radial forces acting on a bubble to interpret the different radial profiles of the gas holdup.

* Corresponding author. Tel.: +86-10-62785464; fax: +86-10-62772051.
E-mail address: wangjf@flotu.org (J. Wang).

1385-8947/$ – see front matter © 2004 Elsevier B.V. All rights reserved.
doi:10.1016/j.cej.2004.01.023

Nomenclature

d	diameter (m)
D	diameter of the pipe (m)
Eo	Eötvös number
Eo_d	modified Eötvös number
F	force per unit volume (N/m^3)
h	distance between probe holes and the distributor (m)
k	turbulent kinetic energy (m^2/s^2)
r	radius (m)
R	radius of the pipe (m)
Re	Reynold number
u	local velocity (m/s)
U	superficial velocity (m/s)
y	distance from the wall (m)

Greek symbols

ε	energy dissipation (W m^3)
ε_g	gas holdup
μ	viscosity (m^2/s)
μ_h	viscosity of pseudo-homogeneous phase $\mu_h/\mu_l = (1 + 0.5\psi_{hs})/(1 - \psi_{hs})^4$ (m^2/s)
ρ	density (kg/m^3)
ρ_h	density of pseudo-homogeneous phase $\rho_h = \rho_l\psi_{hl} + \rho_s\psi_{hs}$ (kg/m^3)
σ	surface tension (N/m)
τ	shear stress (N/m^2)
ψ_{hl}	liquid fraction of pseudo-homogeneous phase
ψ_{hs}	gas fraction of pseudo-homogeneous phase

Subscripts

B	bubble
D	refer to the dispersion force
D, *Eo*	refer to the Eötvös number dependent dispersion force
g	gas phase
H	horizontal
l	liquid phase
L	refer to the lift force
W	refer to the wall force

2. Experimental

The schematic diagram of the experimental setup is shown in Fig. 1. The inner diameter and height of the riser were 0.230 and 4.8 m, respectively. The downcomer, which was connected to the riser 0.2 m above the distributor, has an inner diameter of 0.190 m. The height and diameter of the top section were 0.960 and 0.480 m, respectively.

Air and tap water were used as the gas and liquid phases, respectively. The air was introduced into the system through a porous sinter distributor with holes of diameter 30 μm (case 1) or a perforated plate with holes of diameter 1 mm

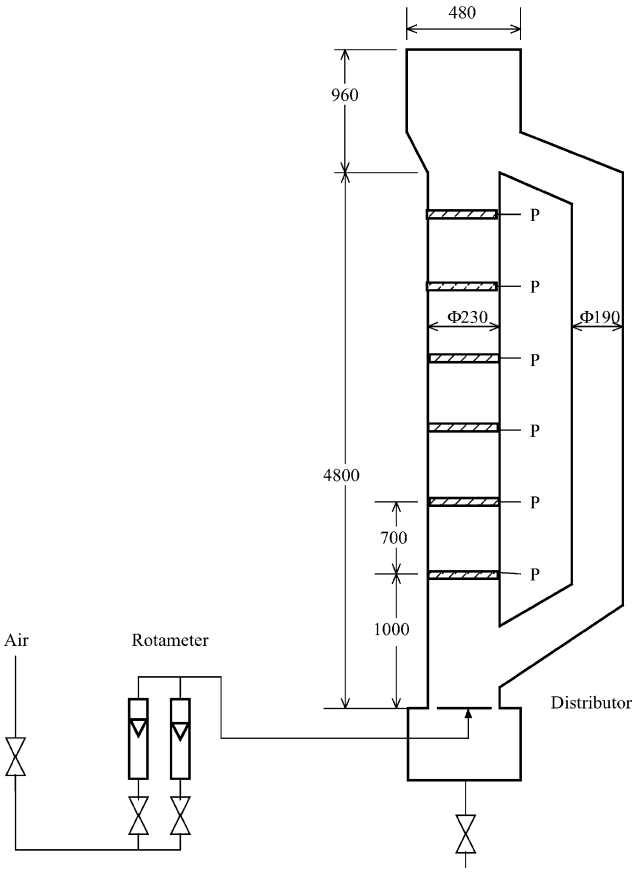

Fig. 1. Schematic representation of the experimental airlift reactor.

and a holed ratio of 0.25% (case 2). The diameter of the distributor is the same as the inner diameter of the riser. The superficial gas velocity, based on the riser cross-section area, varied from 0.008 to 0.032 m/s.

The optic fiber probe was fixed in the wall of the riser, and was movable in the radial direction to measure the radial profiles of the gas holdup, bubble size and bubble rise velocity. Experiments were carried at three different axial positions of 0.8, 2.4 and 4.6 m above the gas distributor in the riser.

3. Measuring techniques

The local gas holdup and the bubble behaviors were measured by a reflective fiber optic probe developed by Wang et al. [23,24]. The probe consists of two parallel optic fibers with a diameter of 62.5 μm. Light reflection occurs at the tip of the optic fibers. The intensity of the reflected light is different when the probe fiber is in the liquid and in a gas bubble. The detected signal is higher when the fiber is in the gas phase. Due to the distance between the two fibers, the output signal from the downstream fiber is a little delayed in time compared to that from the upstream one. The delayed time can be determined by means of the cross correlation method, and the bubble rise velocity can then be calculated

by dividing the distance between the two optic fibers by the time delay. The bubble chord length is calculated by multiplying the bubble signal duration time and the bubble rise velocity. The bubble chord length distribution is obtained through statistical processing, which is transformed to get the bubble size distribution [23]. The bubble frequency, local gas holdup, distribution of the bubble size, and bubble rise velocity are obtained by processing the output signal through algorithms for signal identification, cross correlation and distribution transformation.

4. Hydrodynamic model

Some investigations have been carried out concerning the radial gas profiles in a vertical pipe flow [22,25–27]. Two types of radial profile of the gas holdup, i.e. core-peaking and wall-peaking, were reported. However, core-peaking profile of the gas holdup was much more common, especially in EL-ALRs.

In the present work, we modified the model by Lucas et al. [28] to give a more precise and simple description of the radial profiles of the gas holdup based on the assumption of the equilibrium of the lateral forces acting on a bubble. Three kinds of lateral forces were included: the transverse lift force, the wall lubrication force and the turbulent dispersion force.

It is well known that small bubbles are apt to flow in the near-wall region and present a wall-peaking profile of the gas holdup, whereas large bubbles tend to migrate to the core region and form a core-peaking profile. The migration can be explained with the transverse lift force model proposed by Zun et al. [29] and improved by Tomiyama [30]:

$$F_{\mathrm{L}} = -C_T \rho_{\mathrm{h}} U_{\mathrm{slip}} \frac{\mathrm{d}U_{\mathrm{l}}}{\mathrm{d}r} \tag{1}$$

where

$$C_{\mathrm{T}} = \begin{cases} \min[0.288\tanh(0.121\,Re), 0.00105\,Eo_{\mathrm{d}}^3 - 0.0159\,Eo_{\mathrm{d}}^2 - 0.0204\,Eo_{\mathrm{d}} + 0.474] & \text{for } Eo_{\mathrm{d}} < 4 \\ 0.00105\,Eo_{\mathrm{d}}^3 - 0.0159\,Eo_{\mathrm{d}}^2 - 0.0204\,Eo_{\mathrm{d}} + 0.474 & \text{for } 4 \le Eo_{\mathrm{d}} \le 10 \\ -0.29 & \text{for } Eo_{\mathrm{d}} > 10 \end{cases} \tag{2}$$

$$Eo_{\mathrm{d}} = \frac{g(\rho_{\mathrm{h}} - \rho_{\mathrm{g}})d_{\mathrm{H}}}{\sigma} \tag{3}$$

$$d_{\mathrm{H}} = d_{\mathrm{B}}\sqrt[3]{1 + 0.163\,Eo^{0.757}} \tag{4}$$

where the Reynolds and Eötvös number are calculated by

$$Re = \frac{\rho_{\mathrm{h}} U_{\mathrm{slip}} d_{\mathrm{B}}}{\mu_{\mathrm{h}}} \tag{5}$$

$$Eo = \frac{g(\rho_{\mathrm{h}} - \rho_{\mathrm{g}})d_{\mathrm{B}}^2}{\sigma} \tag{6}$$

Provided that only the lift force given by Eq. (1) is considered, the small bubbles will pass through the pipe wall. A certain constraint is therefore required to prevent the bubble penetration. Antal et al. [31] proposed a wall force that pushes bubbles locating in the near-wall region toward the pipe center. Tomiyama [30] modified their model and gave the constitutive equation for the wall force as follows:

$$F_{\mathrm{w}} = -C_{\mathrm{w}} \frac{d_{\mathrm{B}}}{2}\left(\frac{1}{y^2} - \frac{1}{(D-y)^2}\right)\rho_{\mathrm{h}} U_{\mathrm{slip}}^2 \tag{7}$$

$$C_{\mathrm{w}} = \begin{cases} \exp(-0.933\,Eo + 0.179) & \text{for } 1 \le Eo \le 5 \\ 0.007\,Eo + 0.04 & \text{for } 5 \le Eo \le 33 \end{cases} \tag{8}$$

The turbulent dispersion force considers the smoothing of the radial gas profiles caused by turbulence in a phasic diffusion mechanism. Lahey et al. [32] derived an equation for the turbulent dispersion force per unit volume as

$$F_{\mathrm{D}} = -0.1\rho_{\mathrm{h}} k \frac{\mathrm{d}\varepsilon_{\mathrm{g}}}{\mathrm{d}r} \tag{9}$$

Lucas et al. [28] introduced the second turbulent dispersion force to describe the fluctuating motion caused by the deformation of the bubbles:

$$F_{\mathrm{D},Eo} = -C_{\mathrm{D},Eo}\rho_{\mathrm{h}}(Eo - 1)\frac{\mathrm{d}\varepsilon_{\mathrm{g}}}{\mathrm{d}r} \tag{10}$$

$$C_{\mathrm{D},Eo} = \begin{cases} 0.0015 & \text{for } Eo > 1 \\ 0 & \text{for } Eo < 1 \end{cases} \tag{11}$$

Considering the balance of the lateral forces yields

$$\varepsilon_{\mathrm{g}}(F_{\mathrm{L}} + F_{\mathrm{w}}) + F_{\mathrm{D}} + F_{\mathrm{D},Eo} = 0 \tag{12}$$

The radial of the gas holdup can be calculated from the following equation:

$$0.1k + C_{\mathrm{D},Eo}(Eo - 1)\frac{\mathrm{d}\varepsilon_{\mathrm{g}}}{\mathrm{d}r} + \left(C_{\mathrm{T}} U_{\mathrm{slip}} \frac{\mathrm{d}u_{\mathrm{l}}}{\mathrm{d}r} + C_{\mathrm{w}}\frac{d_{\mathrm{B}}}{2} \times \left(\frac{1}{(R-r)^2} - \frac{1}{(R+r)^2}\right) U_{\mathrm{slip}}^2\right)\varepsilon_{\mathrm{g}} = 0 \tag{13}$$

To solve Eq. (13), the distribution of turbulent kinetic energy is needed. Provided that the liquid velocity has only an axial component, the turbulent energy k satisfies the following balance equation according to the k–ε model:

$$\frac{\mathrm{d}(\rho_{\mathrm{h}} k u_{\mathrm{l}})}{\mathrm{d}r} = \frac{\mathrm{d}((\mu_{\mathrm{t}}/\sigma)(\mathrm{d}k/\mathrm{d}r))}{\mathrm{d}r} + P_k - \rho_{\mathrm{h}}\varepsilon + S_k \tag{14}$$

with the turbulence production term P_k [28]:

$$P_k = \mu_{\mathrm{t}}\left(\frac{\mathrm{d}u_{\mathrm{l}}}{\mathrm{d}r}\right)^2 \tag{15}$$

and the bubble induced turbulence term S_k, which has important impact on the correctness of simulation results [33]:

$$S_k = 0.25(1 + C_{\mathrm{D}}^{4/3})\rho_{\mathrm{h}}\varepsilon_{\mathrm{g}}\frac{U_{\mathrm{slip}}^3}{d_{\mathrm{B}}} \tag{16}$$

Combination of Eqs. (14)–(16) yields the distribution of k. The turbulent viscosity μ_t is calculated using the method given below.

In the vertical pipe flow, the ratio of the shear stress acting on the circumferential surface at r to the wall shear τ_w can be determined from the force balance:

$$\frac{\tau}{\tau_w} = \frac{r}{R} \tag{17}$$

The turbulent viscosity can be determined by the following equation with a given liquid velocity profile, which was measure with the Laser Doppler Velocimeter (LDV) in our previous work [34]:

$$\tau = -(\mu_h + \mu_t)\frac{du_l}{dr} \tag{18}$$

The wall shear stress τ_w is calculated by Brodkey et al. [35]:

$$\tau_w = \tfrac{1}{2} f \rho_h U_l^2 \tag{19}$$

where U_l is the superficial liquid velocity, and f the friction factor which can be determined from the Blasius equation [36]:

$$U_l = \frac{1}{\pi R^2}\int_0^R 2\pi r u_l (1-\alpha_g)\, dr \tag{20}$$

$$f = 0.0791\, Re_h^{-0.25} \tag{21}$$

The radial profile of the gas holdup is calculated by an iterative procedure. The iteration starts from a uniform distribution of the gas holdup, and the radial profiles of turbulent viscosity and turbulent kinetic energy are calculated for this gas holdup profile. Then the radial profile of gas holdup is calculated according to Eq. (13), and is used for a new calculation of the radial profiles of turbulent viscosity and turbulent kinetic energy.

5. Results and discussion

5.1. Influence of the gas distributor

The radial profiles of the gas holdup measured in the developed section with the two types of gas distributor are shown in Fig. 2. It can be seen that the gas holdup increases with the superficial gas velocity.

Core-peaking radial profile of the gas holdup was found in case 2 due to the large bubbles generated by the perforated plate. The gas holdup profiles are relatively flatter in lower superficial gas velocities, and become more and more parabolic with an increase in the superficial gas velocity, Differently, the radial profile of the gas holdup in case 1 was much flatter than that in case 2 in all superficial gas velocities, with a small wall peak at low superficial gas velocities which is more obvious in Fig. 6. This indicates that the porous sinter distributor can distribute the gas phase radially much better than the perforated plate distributor. According

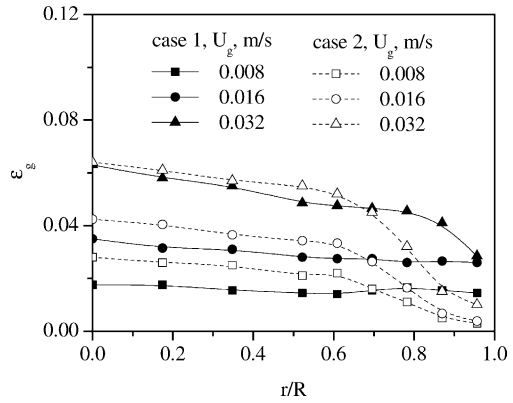

Fig. 2. Comparison of radial gas holdup profiles in case 1 and case 2, $H = 4.6$ m.

to Tomiyama [30], the gas holdup profiles of a gas–liquid system in a vertical pipe can be classified into two types, i.e. the wall-peaking and the core-peaking, depending on the bubble size, therefore the bubble size is a key factor that determines the radial profile of the gas holdup.

It should be pointed out that the wall peaks in case 1 are smaller than that reported by Kataoka et al. [25]. This difference can be attributed to the larger scale of the reactor employed in our study. One the one hand, the velocity gradient in the large-scale reactor is lower [19], therefore the lift force towards the wall is smaller according to Eq. (1). On the other hand, the turbulent fluctuation in a large reactor is much higher than that in the small-scale one, therefore the turbulent dispersion force, which tends to smooth the radial profile of the gas holdup, is larger according to Eq. (9) in a large reactor. The influence of the reactor scale on both the lift force and turbulent dispersion force weakens the wall peak of the gas holdup radial profile in a large scale reactor. The cross-section averaged gas holdup in case 1 is larger than that in case 2 in the same superficial gas velocity, which is due to the smaller bubbles generated by the porous sinter plate.

Fig. 3 compares the bubble sizes between the two cases. In general, the bubble sizes are much smaller in case 1 than in

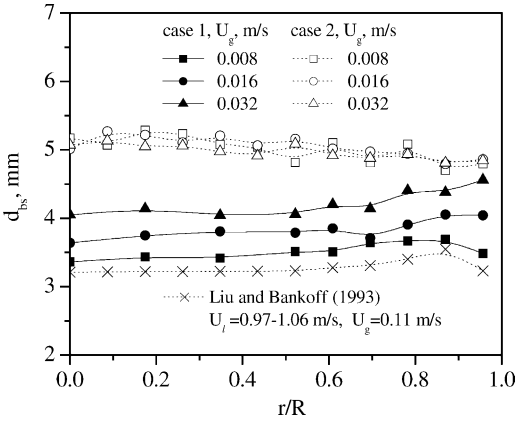

Fig. 3. Comparison of radial profiles of the bubble size in case 1 and case 2, $H = 4.6$ m.

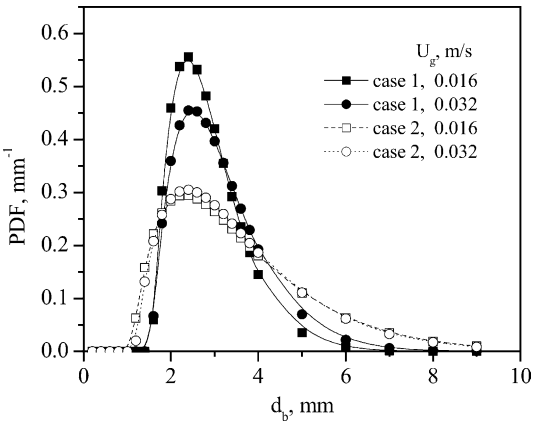

Fig. 4. Comparison of bubble size PDF in case 1 and case 2, $H = 4.6$ m.

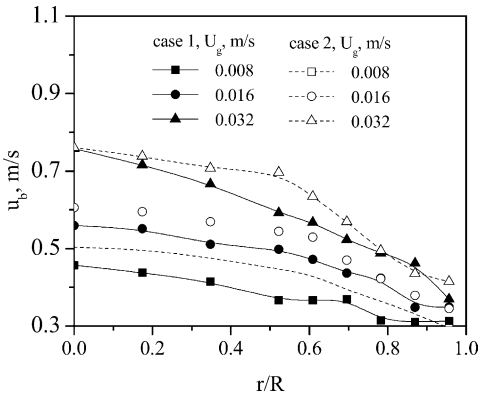

Fig. 5. Comparison of the radial profiles of the bubble rise velocities in case 1 and case 2, $H = 4.6$ m.

case 2 due to the smaller holes in the porous sinter plate, indicating a better distribution performance of the porous sinter plate. In case 1, the bubble size increases with an increase in the superficial gas velocity, which is consistent with the results of Nicol et al. [37]. This is because the initial bubble size generated by the porous distributor increases with an increase in the superficial gas velocity, and the bubble coalescence is also enhanced with increasing bubble numbers. The influence of the superficial gas velocity on the bubble size is not remarkable in case 2. It is shown by Snape et al. [21] that hydrodynamic parameters change little at low gas velocity when distributor hole is between 1 and 3 mm. The radial profiles of the bubble Sauter mean diameter are different for the two cases. In case 1 bubbles near the wall are slightly larger than those in the central region; while in case 2 bubbles in the central region are slightly larger than those in the near-wall region. As discussed earlier, the transverse lift force, the value and direction of which are dependent on the bubble size has influence on the radial movement of bubbles and the radial profile of the bubble size. Another more important influence on the radial profile of the bubble size is the bubble coalescence and breakup. In fact, the bubble size distribution is mainly determined by the equilibrium between bubble coalesce and breakup. This equilibrium is influenced by gas holdup and liquid turbulent kinetic energy dissipation rate. In general, an increase in the gas holdup enhances the bubble coalescence, which in turn causes an increase in the average bubble size. Therefore, the different radial profiles of the gas holdup in cases 1 and 2 are considered to be the main reason for the different radial profile of the bubble size. Similar result was reported by Liu and Banko [38] and Ohnuki and Akimoto [39]. They also found that the bubble size increased towards the wall when the gas holdup had a wall-peaking profile and decreased towards the wall when the gas holdup had a core-peaking profile.

In Fig. 4, the bubble size distributions in the center of the riser are shown. The size distributions have a smaller standard deviation in case 1 than in case 2 due to a better distribution performance of the porous sinter plate. In case 1, the fraction of the large bubbles increases due to the bubble co-

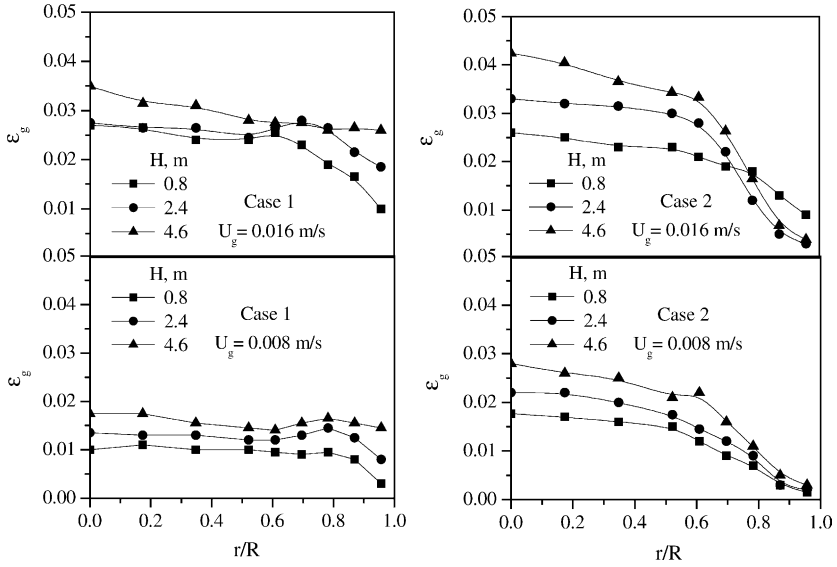

Fig. 6. Axial evolution of the radial profile of the gas holdup in both cases.

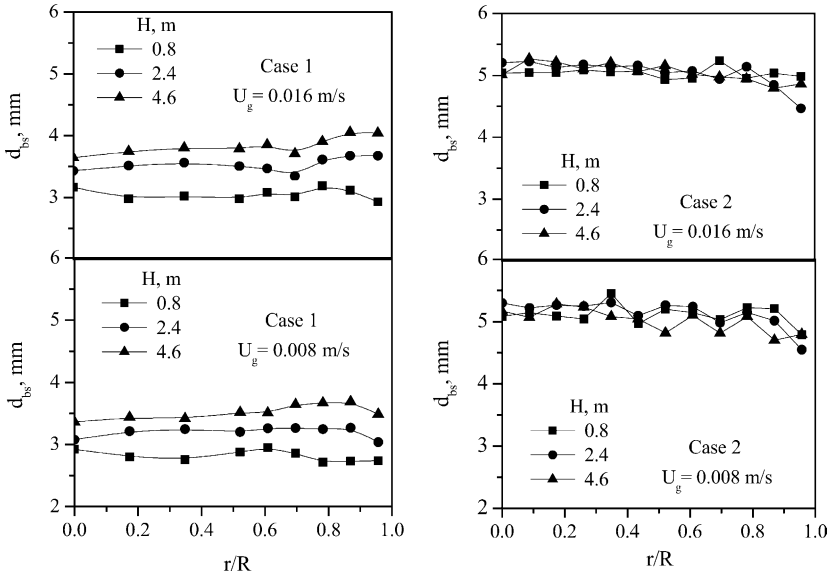

Fig. 7. Axial evolution of the radial profile of the bubble size profiles in case 1.

alescence with an increase in the superficial gas velocity. On the contrary, in case 2 the bubble size distribution does not change remarkably with the superficial gas velocity, which is probably due to the wide distribution of initial bubble size in the distributor region.

The radial profiles of the bubble rise velocity for cases 1 and 2 are shown in Fig. 5. It should be pointed out that the bubble rise velocity in this work is the absolute bubble velocity which equals to the bubble slip velocity plus the local liquid velocity. When the superficial gas velocity increases, the bubble rise velocity increases more remarkably in the central region than in the near-wall region. The bubble rise velocities in case 1 are smaller than that in case 2, especially in the central region, due to the large bubbles in case 2.

5.2. Axial evolution of hydrodynamic parameters

Fig. 6 shows the axial evolution of the gas holdup in both cases. In case 2 the radial profiles of the gas holdup are core-peaking; while in case 1 the gas holdup profiles are much flatter with a small peak near the wall. According to the experiments by Camarasa et al. [40] in a bubble column, the bubbles generated at the distributor were almost had the same size as the bubbles some distance away from the bottom, indicating that the generated bubbles did not coalesce immediately due to the intense turbulence near the distributor region. Therefore, we can conclude that the difference between the two cases is due to different distribution performance of the two types of distributor. The radial profiles of

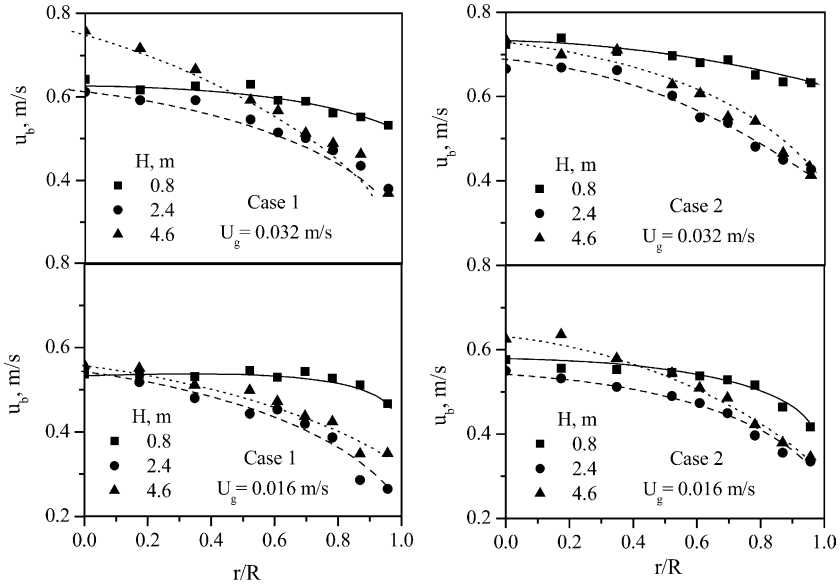

Fig. 8. Axial evolution of the radial profile of the bubble velocity in both cases.

the gas holdup change in both cases along the axial direction: the radial profiles of the gas holdup lose their wall peaks in case 1 and become more and more parabolic in case 2. Based on the model proposed in this work, these changes are mainly due to an increase in the bubble size and a change in the radial profile of the liquid velocity. Under the conditions in this study, bubble coalescence is dominant compared with bubble breakup as the kinetic energy of the turbulent eddies are relatively low. Therefore, in case 1 the bubbles become larger and larger when rising up due to bubble coalescence and gas expansion, as shown in Fig. 7, which in turn weakens the peak near the wall. Wall-peaking profile of the gas holdup in case 1 can hardly be seen near the top of the reactor at the superficial gas velocity of 0.016 m/s. In the system of this work, wall-peaking profile of the gas holdup appears when the bubble Sauter diameter is below 3.7 mm. In case 2, the variation of the bubble Sauter mean diameter along the axial direction are not remarkable, as shown in Fig. 7. This may be due to the wide distribution of the initial bubble size. Therefore, the axial evolution of the gas holdup radial

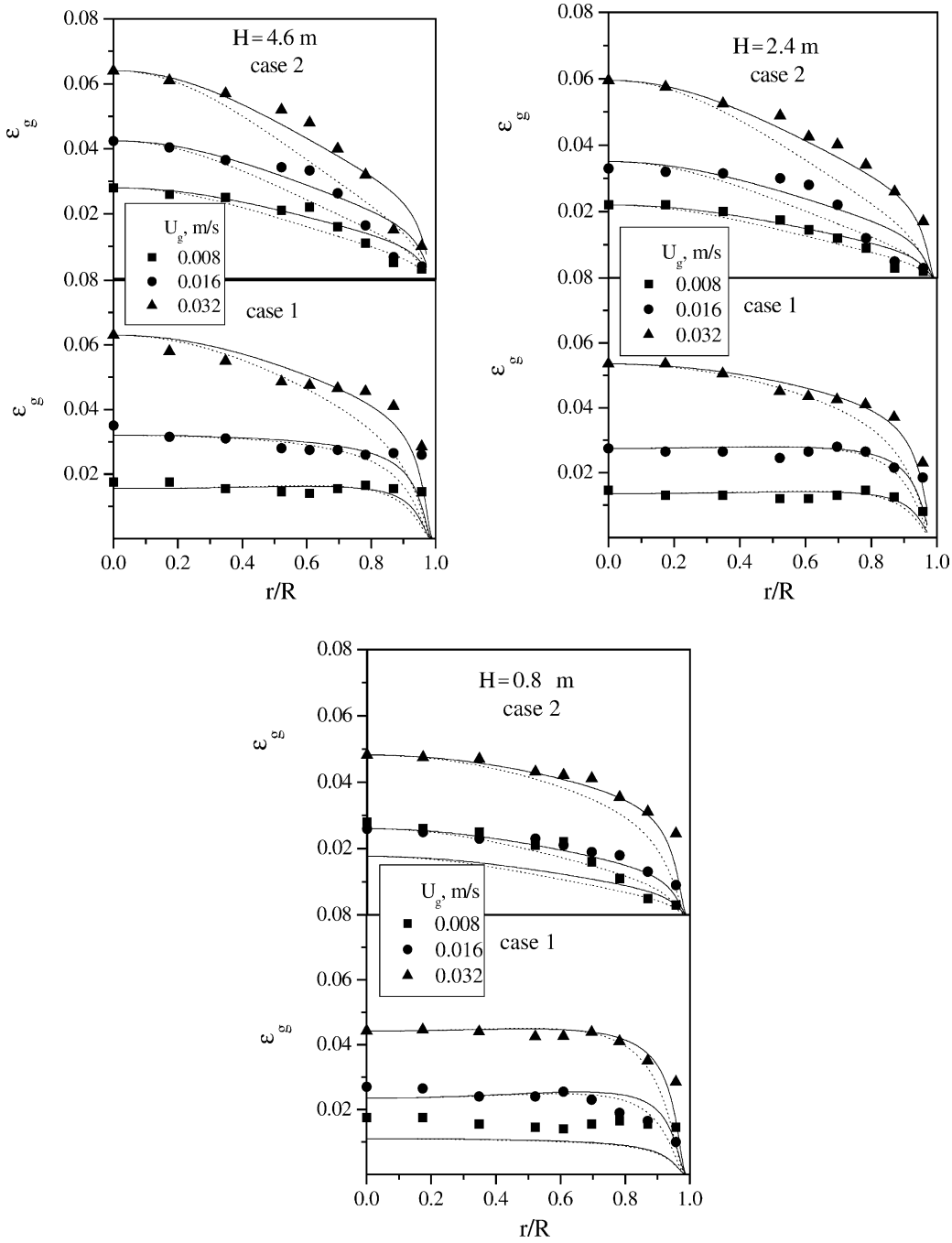

Fig. 9. Comparison of the experimental and the model predicted results in both cases. Symbols: experimental; solid lines: calculated values with S_k; dot lines: calculated values without S_k.

profile is mainly influenced by the liquid velocity, which becomes more parabolic along the axial direction [34].

The axial evolutions of the radial profile of the bubble velocity in both cases are shown in Fig. 8. It can be seen that the difference in the bubble rise velocity in the two cases is not as remarkable as in the gas holdup and bubble size. The bubble velocity is depended on the local liquid velocity and bubble slip velocity. Since the bubble slip velocity changes slightly in the bubble size range of this work, the bubble rise velocity is mainly dependent on the local liquid velocity. The radial profile of the liquid velocity is always parabolic in a gas–liquid vertical pipe flow; therefore the radial profile of the bubble rise is also parabolic as well. From Fig. 8, it can be seen that in both cases the bubble velocities decrease between the height of 0.8 and 2.4 m and then begin to increase. The decrease of bubble velocity at the lower section is caused by liquid acceleration after flow reverse at the reactor bottom, while in the higher section the bubble velocity increases due to an increase in the bubble size caused by bubble coalescence and gas expansion.

6. Model prediction

The predicted radial profiles of the gas holdup in both cases are shown in Fig. 9. A good agreement is obtained between the predicted and measured values, including the core-peaking and the wall-peaking profiles. This agreement confirms the dependence of the lateral forces on the bubble size. From the results, we can see the importance of bubble-induced turbulence term S_k. Good agreement was not obtained when ignoring S_k, as shown by Vial et al. [17] and Lucas et al. [28], who found an inaccuracy of the models due to an underestimate of the turbulence in the k–ε equations.

7. Conclusions

A detailed description of the local hydrodynamic behavior has been obtained in the riser of an external loop airlift reactor with two types of gas distributors: perforated plate and porous sinter plate. The results are valuable for a better understanding of the hydrodynamics in EL-ALRs and can be used for the validation of CFD simulations. It was found that the porous sinter plate could distribute the gas phase much better. Wall-peaking profile of the gas holdup was found in low superficial gas velocities when a porous sinter plate was used as the gas distributor; while core-peaking profile was found in all superficial gas velocity with a perforated plate. It was the different bubble sizes that led to the two types of the radial profile of the gas holdup. Wall-peaking profile of the gas holdup is more obvious in a small-scale reactor due to the larger liquid velocity gradient and less turbulent fluctuation. A model based on the equilibrium of lateral forces acting on a bubble was proposed to describe the radial profiles of the gas holdup and good agreement between the experimental and predicted results was obtained.

Acknowledgements

The authors gratefully acknowledge the financial support by the National Science Foundation of China (No. 20276035).

References

[1] C. Bentifraouine, C. Xuereb, J.-P. Riba, An experimental study of the hydrodynamic characteristics of external loop airlift contactors, J. Chem. Technol. Biotechnol. 69 (1997) 345–349.
[2] R.A. Bello, A characterization study of airlift contactors for applications to fermentations, Ph.D. Thesis, University of Waterloo, Ont., Canada, 1981.
[3] K.H. Choi, W.K. Lee, Circulation liquid velocity, gas hold-up, volumetric oxygen transfer coefficient in external-loop airlift reactors, J. Chem. Technol. Biotechnol. 56 (1993) 51–58.
[4] A.B. Russell, C.R. Thomas, M.D. Lilly, The influence of vessel height and top-section size on the hydrodynamic characteristics of airlift fermentors, Biotechnol. Bioeng. 43 (1994) 69–76.
[5] M.H. Siegel, J.C. Merchuk, Hydrodynamics in rectangular airlift reactors: scale-up and the influence of gas–liquid separator design, Can. J. Chem. Eng. 69 (1991) 465–473.
[6] S. Becker, A. Sokolichin, G. Eigenberger, Gas–liquid flow in bubble column and loop reactors. Part II. Comparison of detailed experiments and flow simulations, Chem. Eng. Sci. 49 (1994) 5747–5762.
[7] M.Y. Chisti, B. Hallard, M. Moo-Young, Liquid circulation in airlift reactors, Chem. Eng. Sci. 43 (1988) 451–457.
[8] A.G. Jones, Liquid circulation in a draft tube bubble column, Chem. Eng. Sci. 40 (1985) 449–462.
[9] Y.C. Hsu, M.P. Dudukovic, Gas holdup and liquid recirculation in gas-lift reactors, Chem. Eng. Sci. 35 (1980) 134–141.
[10] M. Gavrilescu, R.Z. Tudose, Study of the liquid velocity in external-loop airlift reactor, Bioprocess Eng. 14 (1995) 183–193.
[11] J.H. Hills, The operation of a bubble column at high throughputs. I. Gas hold-up measurement, Chem. Eng. J. 12 (1976) 89–99.
[12] M.H. Siegel, J.C. Merchuk, K. Schugerl, Airlift reactor analysis interrelationships between riser, downcomer and gas–liquid behavior, including gas recirculation effects, AIChE J. 32 (1986) 1585–1595.
[13] J.B. Joshi, V.V. Ranade, S.D. Gharat, S.S. Lele, Sparged loop reactors, Can. J. Chem. Eng. 68 (1990) 705–741.
[14] K.H. See, G. Roberts, A.E. Sáez, Effect of drag and frictional loses on the hydrodynamics of gas-lift reactors, AIChE J. 45 (1999) 2467–2471.
[15] M.A. Young, R. Carbonell, D.F. Ollis, Airlift bioreactors: analysis of local two-phase flow hydrodynamics, AIChE J. 37 (1991) 403–428.
[16] M. Utiger, F. Stuber, A.-M. Duquenne, H. Delmas, C. Guy, Local measurements for the study of external loop airlift hydrodynamics, Can. J. Chem. Eng. 77 (1999) 375–382.
[17] C. Vial, S. Poncin, G. Wild, N. Midoux, Experimental and theoretical analysis of the hydrodynamics in the riser of an external loop airlift reactor, Chem. Eng. Sci. 57 (2002) 4745–4762.
[18] A. Ohnuki, H. Akimoto, An experimental study on developing air–water two-phase flow along a large vertical pipe: effect of air injection method, Int. J. Multiphase Flow 22 (1996) 1143–1154.
[19] A. Ohnuki, H. Kamo, H. Akimoto, Developed flow pattern and phase distribution under gas–liquid two-phase flow in a large vertical pipe and prediction of phase distribution by multidimensional two-fluid model, in: Proceedings of Eighth International Topical Meeting on Nuclear Reactor Thermal-Hydraulics (NURETH-8), vol. 3, Kyoto, 1996, pp. 1670–1676.

[20] W.J. McManamey, D.A.J. Wase, S. Raymahasay, K. Thayanithy, The influence of gas inlet design on gas hold-up values for water and various solutions in a loop-type air-lift fermenter, J. Chem. Technol. Biotechnol. 34B (1984) 151–164.
[21] J.B. Snape, J. Zahradník, M. Fialová, N.H. Thomas, Liquid-phase properties and sparger design effects in an external-loop airlift reactor, Chem. Eng. Sci. 50 (1995) 3175–3186.
[22] T. Hibiki, M. Ishii, Experimental study on interfacial area transport in bubbly two-phase flows, Int. J. Heat Mass Transfer 42 (1990) 3019–3035.
[23] T.F. Wang, J.F. Wang, W.G. Yang, Y. Jin, Bubble behavior in gas–liquid–solid three-phase circulating fluidized beds, Chem. Eng. J. 84 (2001) 397–404.
[24] T.F. Wang, J.F. Wang, W.G. Yang, Y. Jin, Experimental study on gas-holdup and gas–liquid interfacial area in TPCFBs, Chem. Eng. Commun. 187 (2001) 251–263.
[25] I. Kataoka, A. Serizawa, Interfacial area concentration in bubbly flow, Nucl. Eng. Des. 120 (1990) 163–180.
[26] E. Krepper, H.-M. Prasser, Measurements and CFX-simulations of a bubbly flow in a vertical pipe, in: Proceedings of the CFX International Users Conference, Friedrichshafen, Germany, June 1999.
[27] M.L. Bertodano, R.T. Lahey Jr., O.C. Jones, Phase distribution in bubbly two-phase flow in vertical ducts, Int. J. Multiphase Flow 20 (1994) 805–818.
[28] D. Lucas, E. Krepper, H.M. Prasser, Prediction of radial gas profiles in vertical pipe flow on the basis of bubble size distribution, Int. J. Therm. Sci. 40 (2001) 217–225.
[29] I. Zun, The transverse migration of bubbles influenced by walls in vertical bubbly flow, Int. J. Multiphase Flow 6 (1980) 583–588.
[30] A. Tomiyama, Struggle with computational bubble dynamics, in: Proceedings of the Third International Conference on Multiphase Flow, ICMF'98, Lyon, France, June 8–12, 1998.
[31] S.P. Antal, R.T. Lahey, J.E. Flaherty, Analysis of phase distribution in fully developed laminar bubbly two-phase: flow, Int. J. Multiphase Flow 17 (1991) 635–644.
[32] R.T. Lahey, M. Lopez de Bertodano, O.C. Jones, Phase distribution in complex geometry conduits, Nucl. Eng. Des. 141 (1993) 177–201.
[33] Y. Sato, M. Sadatomi, K. Sekoguchi, Momentum and heat transfer in two-phase bubble flow. Part I. Theory, Int. J. Multiphase Flow 7 (1981) 167–177.
[34] J. Lin, M. Han, T. Wang, Experimental study on the local hydrodynamic behavior of a three-phase external loop airlift reactor, Ind. Eng. Chem. Res., in press.
[35] R.S. Brodkey, H.C. Hershey, Transport Phenomena—A Unified Approach, McGraw-Hill, New York, USA, 1988, pp. 440–442.
[36] R.H. Perry, D.W. Green, Perry's Chemical Engineer's Handbook, 6th ed., McGraw-Hill, New York, USA, 1984, p. 564.
[37] R.S. Nicol, J.F. Davidson, Gas hold-up in circulating bubble columns, Chem. Eng. Res. Des. 66 (1998) 152–158.
[38] T.J. Liu, S.G. Banko, Structure of air–water bubbly flow in a vertical pipe, Int. J. Therm. Sci. 40 (1993) 1049–1060.
[39] A. Ohnuki, H. Akimoto, Experimental study on transition of flow pattern and phase distribution in upward air–water two-phase flow along a large vertical pipe, Int. J. Multiphase Flow 26 (2000) 367–386.
[40] E. Camarasa, C. Vial, S. Poncin, G. Wild, N. Midoux, J. Bouillard, Influence of coalescence behaviour of the liquid and of gas sparging on hydrodynamics and bubble characteristics in a bubble column, Chem. Eng. Process. 38 (1999) 329–344.